



Proving ligand structure-reactivity correlation on multinuclear copper electrocatalysts supported on carbon black for the oxygen reduction reaction

Ricardo Venegas^{a,b}, Karina Muñoz-Becerra^c, Sophie Juillard^b, Lin Zhang^b, Rubén Oñate^a, Ingrid Ponce^a, Vincent Vivier^{b,d}, Francisco J. Recio^{e,*}, Carlos M. Sánchez-Sánchez^{b,*}

^a Facultad de Química y Biología, Universidad de Santiago de Chile, Av Libertador Bernardo O'Higgins, Estación Central, Región Metropolitana, Santiago 3363, Chile

^b CNRS, Laboratoire Interfaces et Systèmes Electrochimiques (LISE), Sorbonne Université, 4 Place Jussieu, Paris 75005, France

^c Centro Integrativo de Biología y Química Aplicada (CIBQA), Universidad Bernardo O'Higgins, General Gana 1702, Santiago 8370854, Chile

^d Laboratoire de Réactivité de Surface (LRS), Sorbonne Université, CNRS, UMR 7197, Paris 75005, France

^e Departamento de Química Física Aplicada, Facultad de Ciencias, Universidad Autónoma de Madrid, C/Francisco Tomás y Valiente 7, Madrid 28049, Spain

ARTICLE INFO

Keywords:

Multicopper electrocatalysts
Oxygen reduction reaction
SECM
Structure reactivity correlation

ABSTRACT

Bioinspired transition-metal catalysts seek to mimic the specific active site of metalloenzymes, as the multicopper oxidase, that can efficiently reduce dioxygen to water via a complete 4-electrons mechanism at low overpotential. However, the multicopper oxidase enzymes lack stability under operando conditions, hampering their application in fuel cell electrodes. Bioinspired multicopper catalysts present a remarkable electrocatalytic activity for the oxygen reduction reaction (ORR), where the structure and electronic properties of the ligands play a fundamental role. In this work, we explore the instantaneous catalytic activity and its evolution under operando conditions of two multicopper catalysts with different ligand flexibility, pyridyl ligand (CuL1), and pyridylmethyl ligand (CuL2), by conventional electrochemical techniques and scanning electrochemical microscopy (SECM). Both catalysts present similar instantaneous electrocatalytic activity with no significant role of the ligand, but there is a change in the mechanism. While the rigidity of CuL1 reduces the dioxygen via direct 4e⁻, the catalyst with higher flexibility (CuL2) follows a 2e⁻ × 2e⁻ mechanism. The production of H₂O₂ as ORR byproduct evaluated by rotating ring-disk electrode (RRDE) and stability test evaluated under ORR operating conditions by SECM imaging of both catalysts demonstrated a higher decrease in catalytic activity and higher H₂O₂ production in CuL2 than in CuL1, which evidences a ligand structure-reactivity correlation. These results contribute to the rational design of next generation of copper catalysts and open the door to a new methodology to evaluate the activity evolution under operando conditions by SECM.

1. Introduction

The development of durable, efficient, and low-cost oxygen reduction reaction (ORR) catalysts to replace the scarce and expensive noble metal-based electrodes in energy conversion devices considers the use of earth-abundant elements such as first-row transition-metals ($M = \text{Fe, Co, and Cu}$, among others) [1,2]. Bioinspired transition-metal catalysts mimic the specific active site of metalloenzymes that can efficiently reduce dioxygen to water via a complete 4-electron mechanism [3]. Systematic studies of bioinspired molecular catalysts, such as MN4 metal-phthalocyanines and porphyrins, have contributed to determine theoretical and experimental reactivity descriptors as guidance to

optimize the rational design of new catalysts for ORR, including correlations of $M(\text{III})/M(\text{II})$ formal potential and catalytic activity (j) with d -electrons metal, donor-acceptor intermolecular hardness, and $M\text{-O}_2$ binding energy, among others [4–6]. Those descriptors have evidenced that the chemical structure of the ligand tunes the ORR activity since it modulates the electronic structure of the active metal site within the molecular catalyst. Moreover, the nature of the ligand also plays an important role in the successful immobilization of the molecular catalyst on carbon-based materials by modulating the strength of the established π -interactions [7,8].

Biomimetic copper-based catalysts for ORR are an interesting alternative to platinum group metal catalysts [9]. Many multicopper oxidase

* Corresponding authors.

E-mail addresses: javier.recio@uam.es (F.J. Recio), carlos.sanchez@sorbonne-universite.fr (C.M. Sánchez-Sánchez).

<https://doi.org/10.1016/j.electacta.2022.141304>

Received 25 July 2022; Received in revised form 3 October 2022; Accepted 4 October 2022

Available online 5 October 2022

0013-4686/© 2022 The Authors. Published by Elsevier Ltd. This is an open access article under the CC BY license (<http://creativecommons.org/licenses/by/4.0/>).

enzymes can naturally bind, cleavage, and reduce dioxygen molecules to water at low overpotential [10,11]. However, their large molecular size and lack of stability under *operando* conditions hamper their direct application in fuel cell electrodes [12,13]. Nevertheless, these enzymes have inspired the synthesis of different copper molecular catalysts exhibiting high activity for ORR [9,14]. In particular, studies conducted with mononuclear copper complexes synthesized with chelating ligands, such as 1,10-phenanthrolines (phen) [6,15,16] and tris(2-pyridylmethyl) amine (tropa) [17,18], reveal that the stability of those copper-based catalyst relies on the properties of the ligands. In this sense, ligands should be capable of holding and facilitating the Cu(II)-square-planar \rightleftharpoons Cu(I)-tetrahedral conformational transition associated with the Cu(II)/Cu(I) redox process to avoid demetallation during the ORR [6,9,19]. In contrast, if the ligand structure is too rigid, as in the case of Cu(II)-phthalocyanines and -porphyrins, the ligand stabilizes the Cu(II) redox state, and the complexes are almost inactive [7,20,21]. Consequently, the rigidity of the ligands could be considered detrimental to their catalytic activity, while the ligand's lability increases their ORR activity, favoring the formation of vacancies in the Cu(I) active site for the adsorption of the dioxygen molecule [16,17,22–24].

As for MN4-type catalysts [25–28], the Cu(II)/Cu(I) formal potential of Cu-(phen)₂ mononuclear complexes has been established as an ORR reactivity descriptor, showing an increase in the catalytic activity with a more positive formal potential, that is reached by adding electron-withdrawing substituents over the peripheral sites of (phen) ligand [6]. However, multinuclear copper-based molecular catalysts present higher activity and selectivity towards the ORR than mononuclear-copper complexes [29–32]. Even though the Cu(II)/Cu(I) formal potentials of mono- and bi-nuclear catalysts evidence similarities, binuclear catalysts generate a lower amount of hydrogen peroxide (H₂O₂) than the mononuclear ones, revealing that the binuclear arrangement favors the selectivity of the catalyst towards the 4-electron pathway via the formation of (Cu₂-O₂) dimer intermediates, as it was demonstrated by Tse et al. [33]. One of the most active multicopper catalysts reported so far has been synthesized using 3,5-diamino-4-*H*-1,2,4-triazole ligands (Hdatrz) and Cu(II) salts (*E*_{onset} = 0.73 V vs. RHE, pH 7 with a high selectivity) [29,34]. Following these results, Xi et al. [30] synthesized a bimetallic copper complex rGO-TAPDPyCu covalently attached to a graphene substrate using a substituted 1*H*-1,2,3-triazole ligand that catalyzes the ORR efficiently via 4-electrons mechanism with an onset potential of 0.95 V vs. RHE at pH 13, being one of the top Cu-based binuclear ORR catalysts. These advances demonstrated the potential of triazole derivatives as ligands for Cu-based catalysts. In [30,35,36], particular, the bidentate 4-substituted-3,5-(2-pyridyl)-1,2,4-triazole and related ligands have led to the synthesis of bi- and multinuclear systems with different transition metals [35,37]. However, most of the complexes obtained with those ligands present poor crystallinity (limiting their crystalline structures resolution) [38] and the synthesis conditions are determinant for their nuclearity, varying from mono- to multinuclear- structures and including mixtures of both [37,

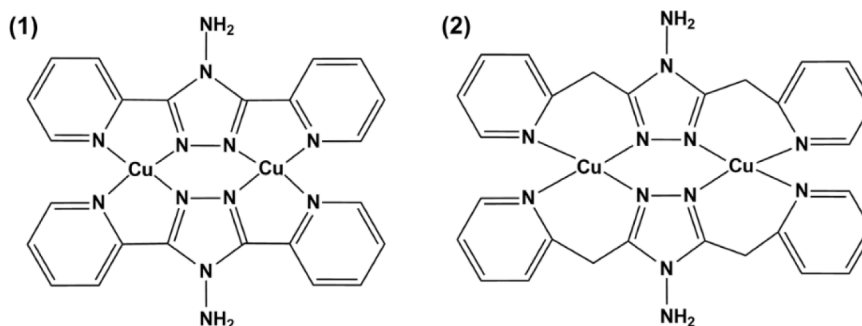
39,40].

Therefore, the correct design of the ligands is critical to adequately improving the efficiency and stability of bioinspired copper-based catalysts immobilized on electrode surfaces [9]. In this study, we evaluate the catalytic activity and stability for ORR of two multinuclear Cu-based catalysts (CuL1) and (CuL2) supported on carbon black, paying special attention to the impact on the reactivity of the structural properties of the synthesized ligands: L1 = 4-amino-3,5-bis(2-pyridyl)-1,2,4-triazole and L2 = 4-amino-3,5-bis(2-pyridylmethyl)-1,2,4-triazole. The main difference between both ligands is the presence of a methyl linker between the pyridyl and triazole moieties in L2 (Scheme 1). The inclusion of this methyl group was considered strategically to increase the flexibility of the ligand. This type of pyridylmethyl-substituted ligand has not been evaluated before and could facilitate the conformational redox transition from Cu(II) to Cu(I) and increase the stability of the catalyst in *operando* conditions. Thus, rotating ring-disk electrode (RRDE) for evaluating the product selectivity during ORR, together with local electrocatalyst interrogation techniques such as scanning electrochemical microscopy (SECM) [41–45], are used here for studying the ligand structure-reactivity correlation under realistic reaction conditions. The SECM is based on the steady-state diffusion-controlled regime provided by either an ultramicroelectrode (UME) or a micropipette and has already demonstrated its utility for studying ORR using different operation modes [46–52]. The activity evaluation of different catalytic materials has been extensively reported by SECM [53]. Some of them have been devoted to evaluate the activity of immobilized molecular electrocatalysts [54–57], and others to identify the reactive intermediate species generated during electrocatalysis [58]. However, to the best of our knowledge, none has been focused on the activity evolution in *operando* conditions. For that purpose, a micropipette-based mode of SECM is employed here, the pumped micropipette delivery/substrate collection (pumped-MD/SC) mode, which allows quantitative catalytic activity evaluation by locally injecting a controlled O₂ saturated solution flow in close vicinity of the copper-based catalysts under study. The micropipette is connected through a Teflon capillary to a microliter syringe pump, which controls the injection flow. This pumped-MD/SC mode was initially developed for pitting corrosion studies [59–62], and this article represents one of the first examples where it is successfully adapted for electrocatalyst evaluation.

2. Experimental

2.1. Synthesis and characterization of Cu-catalysts

Scheme 1 shows the two different multinuclear units proposed for the copper catalysts synthesized with the ligands (L1) 4-amino-3,5-bis(2-pyridyl)-1,2,4-triazole and (L2) 4-amino-3,5-bis(2-pyridylmethyl)-1,2,4-triazole. Both ligands were obtained by solvothermal synthesis following a procedure previously reported in literature [63] and their characterization was performed by ¹H NMR and ¹³C NMR in DMSO-*d*₆



Scheme 1. Proposed binuclear units for Cu-catalysts with ligand L1: 4-amino-3,5-bis(2-pyridyl)-1,2,4-triazole ((1) CuL1) and L2: 4-amino-3,5-bis(2-pyridylmethyl)-1,2,4-triazole ((2) CuL2).

(Figures S1-S4). (L2) exhibits an extra signal with respect to (L1) at 4.28 ppm corresponding to the methyl bridge between the triazole and pyridine moieties (Figure S3). Both copper-based catalysts were prepared by precipitation as follows: A solution of the corresponding ligand (1.0 mmol) dissolved in CH₃CN was added dropwise to a solution containing the Cu (I) precursor tetrakis(acetonitrile) copper (I) perchlorate [Cu(CH₃CN)₄]ClO₄ (1.0 mmol) in CH₃CN under Ar atmosphere. The mixture was stirred during 1 h at room temperature. Then, the solvent was eliminated on a rotary evaporator, obtaining a brown solid that was purified by solvent evaporation. The units of CuL1 and CuL2 shown in Scheme 1 were proposed in base of the elemental analysis combined with TXRF (Total Reflection X-ray Fluorescence) characterization showing a Cu:N ratio of 1:6, which agrees with a 1:1 Cu:L ratio (see Supplementary Materials).

2.2. Electrochemical measurements

The electrochemical characterization and the electrocatalytic activity studies performed by cyclic voltammetry (CV), linear sweep voltammetry (LSV) and chronoamperometry (CA) were conducted with a BASI EPSILON (Bioanalytical System) or a CHI 760E (CH Instruments) potentiostat in a conventional electrochemical cell, using a three-electrode configuration at room temperature with or without working electrode rotation. The working electrode was a 4 mm diameter glassy carbon (GC) disk electrode (PINE Instruments®), where a catalytic ink was deposited. A Pt wire (0.5 mm in diameter) and an Ag/AgCl_{KCl sat} electrode placed within a Luggin capillary were used as counter and reference electrodes, respectively. Potentials reported here were converted to reversible hydrogen electrode (RHE) using the relation: $E_{\text{RHE}} = E_{\text{Ag/AgCl}} + 0.197 + 0.059 \text{ pH}$. To modify the GC electrode surfaces, two different catalytic inks were prepared by dispersing 1 mg of the catalyst (CuL1 or CuL2) and 4 mg of carbon Vulcan XC-72R (carbon black from Cabot Co.) in 5 mL of isopropanol:water (1:4 v/v) and 20 μL of Nafion (5 wt.% in alcohols, Sigma-Aldrich) under sonication for 30 min. GC electrodes were modified by spin coating, dropping 10 μL of the catalytic inks onto electrode surface and drying under nitrogen flow. The solution composition was either Ar- or O₂-saturated 0.1 M NaClO₄ and 0.04 M Britton-Robinson buffer adjusted to pH 5.0. All solutions were prepared with ultrapure Mili-Q water (18.2 M Ω cm).

CVs, LSVs and CAs using the rotating ring-disk electrode (RRDE) (PINE Instruments®) (GC disk, diameter 4 mm and geometrical area: 0.126 cm²; Pt ring, RRDE collection efficiency 0.420) were performed at different rotation rates for evaluating the catalytic kinetic parameters, Tafel slopes, the number of electrons transferred (n) and amount of H₂O₂ produced during the ORR. In particular, H₂O₂ quantification was obtained from LSV curves at a low scan rate, 5 mV/s, to allow ORR steady-state conditions on the catalytic ink; meanwhile, the Pt ring potential was held at a constant value of 1.2 V vs. RHE where the H₂O₂ generated at the catalyst is collected by oxidation under diffusion-controlled conditions. An O₂-saturated 0.1 M NaClO₄ and 0.04 M Britton-Robinson buffer solution adjusted to pH 5.0 was used for that purpose. The (n) value and the H₂O₂ percentage produced during ORR were calculated using Eqs. (1) and (2).

$$n \text{ of electrons} = 4 \frac{I_d}{I_d + \frac{I_r}{N}} \quad (1)$$

$$\% \text{H}_2\text{O}_2 = \frac{100 * \frac{2I_r}{N}}{(I_d + \frac{I_r}{N})} \quad (2)$$

Where the terms I_d and I_r correspond to disk and ring currents, respectively. N is the experimental RRDE collection efficiency value, 0.42 in this case.

2.3. Scanning electrochemical microscopy (SECM)

2.3.1. Active sites normalization and multi-sample preparation

The catalytic inks for SECM were prepared following the procedure described above but changing the catalyst-to-carbon black mass ratio to 1:1. Thus, 1 mg of the catalyst (CuL1 or CuL2) and 1 mg of carbon Vulcan XC-72R (carbon black from Cabot Co.) were dispersed in 2 mL of isopropanol:water (1:4 v/v) under sonication for 30 min. The quantification of active catalytic sites present on both Cu-catalysts inks was determined by CV in Ar-saturated 0.1 M NaClO₄ and 0.04 M Britton-Robinson at pH 5.0 by varying the amount of catalytic ink deposited on the electrode and evaluating the charge contained in the oxidation peaks displayed between 0 and 1.1 V vs RHE (see Figure S5). Then, the most concentrated ink was diluted to exhibit an equal amount of active catalytic sites per dispersion volume in both cases ($4.0 \times 10^{-11} \pm 0.2 \times 10^{-11} \text{ mol } \mu\text{L}^{-1}$). These catalytic inks were separately deposited on a flat GC plate ($1.5 \times 1.5 \text{ cm}^2$) using a picoliter solution dispenser CHI 1550A (CH Instruments). A total of 120 drops of each catalytic ink were dispensed in individual spot samples on the GC plate, allowing the solvent to be evaporated before adding 1 μL of Nafion (5 wt% solution) to ensure proper interaction between the ink and the GC current collector plate. The average spot size obtained was 270 μm in diameter.

2.3.2. Glass micropipette fabrication

Micropipettes were prepared by pulling borosilicate capillaries with O.D.: 1.0 mm and I.O. 0.5 mm and length 15 cm (World Precision Instruments) using a CO₂ laser-based puller P-2000 from Sutter Instrument Co. Micropipettes with an internal opening diameter of c.a. 20 μm were fabricated. The micropipette opening diameter was measured using an optical metallographic microscope BA310MET-H (Motic Co.) (Figure S6). Then, those glass micropipettes were loaded with an O₂-saturated electrolyte solution and connected through a PTFE capillary to a syringe before starting the electrocatalyst evaluation by SECM.

2.3.3. Scanning electrochemical microscopy analyses

Two SECM experiments are reported here: i) SECM imaging and ii) SECM activity quantification by chronoamperometry. A CHI 920D (CH Instruments) microscope in the pumped micropipette delivery/substrate collection mode (pumped-MD/SC) was used in all cases. In this mode configuration, a borosilicate micropipette with an internal opening diameter of 20 μm replaces the UME to locally deliver the analyte of interest (O₂) in the vicinity of the electrode surface. The top-end of the glass micropipette was connected to a 300 μL Terumo® syringe filled with an O₂-saturated 0.1 M NaClO₄ and 0.04 M Britton-Robinson buffer solution at pH 5.0. A KD Scientific® microfluidic syringe pump was used to release the solution from the syringe into the micropipette gradually and subsequently in the vicinity of the electrode surface at a controlled flux rate (55 $\mu\text{L h}^{-1}$), as described elsewhere [59–62]. The electrochemical cell was built in Teflon with an 8 mm diameter aperture at the bottom; the GC substrate containing the two Cu-based catalytic spots under study was placed in the cell to allow the catalytic spots to be in contact with the electrolyte solution. An Ag/AgCl_{KCl sat} in a Luggin capillary and a Pt wire (0.5 mm in diameter) were used as a reference and counter electrodes, respectively. The same solution contained within the glass micropipette, but without the presence of O₂ (Ar-saturated), was used in the electrochemical cell. Then, before all SECM experiments, the tilt of the substrate electrode was canceled by successive approach curves on three different locations using an UME in the feedback mode. This allows keeping the tilt of the substrate at $\Delta z/\Delta x$ (or Δy) $\leq 1.5 \mu\text{m/mm}$ [64]. Then, the solution in the electrochemical cell was dried out, and the UME was replaced by the micropipette filled up with the O₂-saturated electrolyte and connected to a microfluidic syringe pump. The precise positioning of the micropipette was performed by an approach curve from air to a point of contact on the GC substrate electrode, meanwhile the solution was pumped through the micropipette. The contact point was established by physical contact between the

meniscus formed at the apex of the micropipette and the GC plate in the air. This technique avoids damaging the micropipette integrity and allows high sensitivity to position the micropipette in the close vicinity of the substrate. Finally, the micropipette-substrate distance was set up at 50 μm , and the electrochemical cell was filled up with the Ar-saturated electrolyte.

(i) **SECM imaging.** The potential of the Cu-based catalytic spots deposited on the GC substrate electrode was held constant at a proper potential value to evaluate ORR activity; meanwhile, the micropipette scans the substrate electrode pumping out a controlled flow of O_2 -saturated electrolyte solution ($55 \mu\text{L h}^{-1}$). Then, the oxygen reduction current produced at the substrate during the micropipette scan in the X-Y plane was recorded as a function of micropipette position and plotted as a SECM image. An argon blanket was kept over the Ar-saturated 0.1 M NaClO_4 and 0.04 M Britton-Robinson at pH 5.0 solution during the experiment to keep the solution free from atmospheric oxygen. Consecutive SECM images of the same electrode at the same potential are useful for evaluating the ORR activity evolution in operando conditions. Thus, consecutive SECM images were recorded varying the applied potential every 0.1 V in a range of 0.194 V to 0.794 V vs. RHE.

(ii) **SECM activity quantification by chronoamperometry.** This experiment was conducted with the micropipette in static mode by individually addressing each catalytic spot. The micropipette was placed at the center of the catalytic spot under study at a micropipette-substrate distance of 50 μm . Then, a chronoamperometry for 270 s keeping the potential of the Cu-based catalytic spot deposited on the GC electrode constant in an active region for ORR was carried out. Firstly, the

substrate background current was collected during 90 s; meanwhile, the micropipette was not delivering any O_2 in solution ($I_{\text{background}}$) because the syringe pump was turned off. Secondly, the syringe pump was turned on and an O_2 -saturated electrolyte solution flow was delivered from the micropipette during the next 90 s and the substrate current collected corresponds to the ORR activity at the catalytic spot (I_{ORR}) under steady-state conditions. Finally, the syringe pump was turned off again for 90 s more before the end of the chronoamperometry experiment to recover the background current. Then, the net ORR current (ΔI) associated with the activity of each catalytic spot studied was calculated from the difference between the reduction current in the presence and the absence of O_2 ($\Delta I = I_{\text{ORR}} - I_{\text{background}}$) at different applied potentials.

3. Results and discussions

The synthesized L1 and L2 ligands are capable of leading to mono- and/or multi-nuclear Cu complexes [37,40]. The basic catalytic unit [CuL] could form dimers and oligomers where the Cu centers are bridged in a N1-N2 coordination mode by the triazole ligands forming binuclear Cu complexes [30,39,40]. The characterization by elemental analysis and TXRF of the synthesized Cu catalysts, CuL1 and CuL2, show a nitrogen-to-copper ratio close to 6:1 for both catalysts, which is compatible with the coordination of one ligand per Cu atom (see Scheme 1 and supplementary materials) and seems to indicate the formation of pure binuclear Cu units. However, this is not the case here and both CuL1 and CuL2 catalysts correspond to a mixture of mono- and bi-nuclear Cu complexes. The electrochemical characterization of the

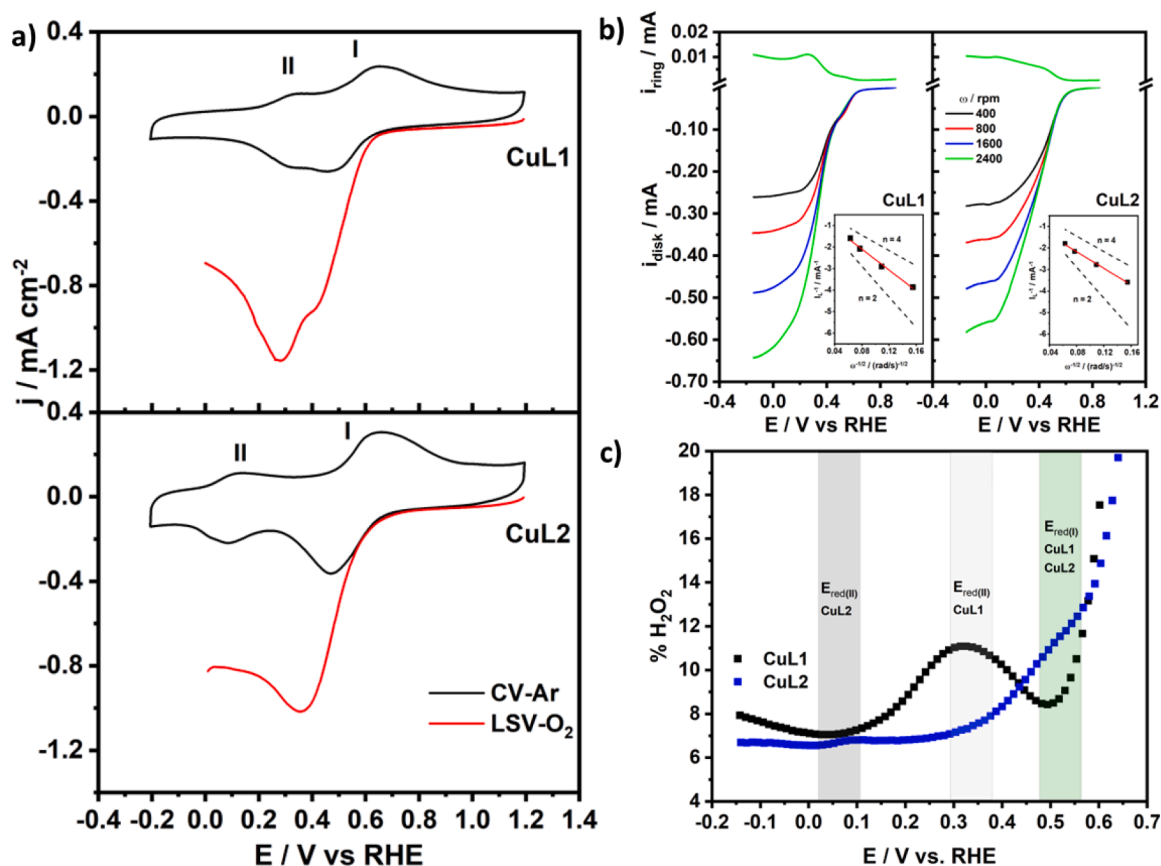


Fig. 1. (a) Electrochemical characterization of CuL1 y CuL2 catalysts in 0.1 M NaClO_4 and 0.04 M Britton-Robinson buffer solution at pH 5.0 under Ar atmosphere by CV (black lines) and the polarization curves (LSV) under O_2 -saturated solution without rotation (red lines). LSV and CV scan rates = 0.050 V s^{-1} . (b) The RRDE polarization curves of CuL1 and CuL2 catalysts in O_2 -saturated 0.1 M NaClO_4 and 0.04 M Britton-Robinson buffer solution at pH 5.0. (scan rate = 0.005 V s^{-1} , Pt ring potential held at 1.2 V vs. RHE). Inset: Koutecky-Levich plots. (c) H_2O_2 production from disk and ring currents displayed at 1600 rpm. The reduction Cu(II)/Cu(I) potentials of the first and second processes of each catalyst are highlighted. (For interpretation of the references to color in this figure, the reader is referred to the web version of this article).

two catalysts performed by cyclic voltammetry probes the coexistence of mono- and bi-nuclear Cu moieties. Fig. 1a shows the CVs of CuL1 and CuL2 catalysts in an O₂-free electrolyte solution (black plots). Two faradaic processes identified as (I) and (II) appear in Fig. 1a, which correspond to Cu(II)/Cu(I) faradaic processes of two differentiated copper centers [65]. For purely synthesized binuclear Cu complexes, a single faradaic process in CV has been widely reported in the literature due to the symmetry of those complexes [66]. Nevertheless, Cu(II)-Cu(I) mixed-valence complexes have been also reported in pure binuclear copper complexes in organic solvents [67]. The first process (I), at more positive values, presents a quasi-reversible behavior that could be associated with bi-nuclear sites, since it is associated with the reorganizational energy attributed to the structural changes of the Cu centers during the electron-transfer process from Cu(II)(square-planar) to Cu(I) (tetrahedral), which are hampered by the binuclear structure [30]. Process (II) also presents a quasi-reversible behavior, indicating a different structure of the copper center, mainly mononuclear centers, that can be part of the defects or terminal structures in a multicopper system [33,65] where each Cu site will be coordinated to one ligand completing its coordination environment with stabilizing anions. For this type of mononuclear units, the reorganization energy is expected to be lower since their conformational change is less hindered by the coordination environment since they correspond to terminal mononuclear Cu sites anchored between the pyridyl moiety and the triazole core. The differences between CuL1 and CuL2 (II) redox peaks arise from the rigidity related to the ligands, in the case of the CuL1 catalyst, the pyridyl moiety is directly linked to the triazole core, restricting the conformation change associated with the Cu(II)/Cu(I) redox process in a similar way to the steric effect evidenced by Cu-2,9-substituted-1,10-phenanthrolines [6] shifting the redox potential towards more positive values. For CuL2, the pyridyl moiety is linked to the triazole core by a methyl group that confers higher flexibility than CuL1. These assignments are in agreement with theoretical and experimental calculations, where the increase in the steric impediment shifts the redox potential of the copper centers in CuN4 structures to more positive values [6]. Moreover, the appearance of redox processes for mononuclear Cu entities at more negative potential values than for multinuclear systems has been already demonstrated [33]. In contrast, the attribution of those two faradaic processes shown in Fig. 1a to the immobilization of one single type of Cu catalyst on different active sites of underlying carbon substrate, as previously reported on multiwalled carbon nanotubes [68], is not justified on this case due to the large potential gap between the two peaks. In addition, the surface coverage of each Cu-based catalyst was calculated from the charge involved in the oxidation peaks observed in Fig. 1a (black plots). For both catalysts, the amount of active sites is in the same order of magnitude (Table 1), as well as the amounts related to the binuclear and mononuclear sites (10^{-8} mol cm⁻²). Furthermore, the ratio of binuclear to mononuclear sites was estimated in 2.6 for CuL1 and 1.8 for CuL2, with the binuclear sites being the majority in terms of surface coverage (Table S1).

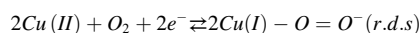
Fig. 1a also shown the linear polarization curves obtained in O₂-saturated electrolyte solution under non-rotating conditions (red lines). The CuL1 polarization curve presents two current waves before the mass transfer region, respectively, at low and high overpotentials. These

waves take place at potential values close to the faradaic process detected by CV for both copper centers. However, for the CuL2 complex, the second wave is undetectable since the potentials related to the second faradaic process are in the mass transfer region. For both catalysts, the onset potential of the ORR is linked to the first Cu(II)/Cu(I) redox potential (binuclear copper centers), indicating that the electro-generated Cu(I) of binuclear centers during the polarization acts as the most active site for the ORR, and follow an inner-sphere mechanism as previously proposed in the literature [9,19].

Fig. 1b shows the RRDE catalytic tests on CuL1 and CuL2 catalysts at different rotating rates (400–2400 rpm). The disk currents have been corrected from the capacitive current determined by CV tests at the same scan rate. Both catalysts present a similar onset potential close to 0.64 V vs. RHE and are in the range of other multicopper complexes [9]. The product selectivity for the ORR was monitored by the ring currents collected during the polarization curves. As is shown in Fig. 1c, for the CuL1 catalyst, there is an apparent increase in the H₂O₂ production at potentials values close to the reduction potential of the mononuclear active sites (0.3 – 0.4 V), which corroborates the presence of a residual mononuclear complex at the electrode surface. In addition, the lower production of H₂O₂ at low overpotentials indicates the high selectivity via direct 4-electron reduction to H₂O of binuclear active sites of CuL1 catalysts. Unlike the CuL2 catalyst, the highest production of H₂O₂ was detected at low overpotentials, in the potential range where the binuclear active sites catalyze the ORR. Since the H₂O₂ production is above 10% there, the ORR mechanism could be associated with a 2e⁻ x 2e⁻ mechanism with the initial formation of H₂O₂ [9]. This mechanism change comparing CuL1 and CuL2 catalysts is related to the methyl group present in the ligand L2, since it seems to destabilize the adsorption of the peroxide intermediate Cu-OOH that can be desorbed during the ORR. This fact could be detrimental in operando conditions since the generation of H₂O₂ directly corrode the carbon matrix or could degrade the catalyst via Fenton reaction by forming hydroxyl radicals.

The number of electrons transferred (*n*) during the ORR was determined simultaneously from Koutecký-Levich (K-L) analysis [69] (Fig. 1b-inset) and from the H₂O₂ quantification by RRDE using Eq. (1) (Figure S7). The *n* value calculated by K-L plots is in the range of 3 to 3.7 and is lower than the calculated from Eq. (1), which is in the range of (3.8 - 3.9) for both catalysts. These values are summarized in Table 1. This difference probably implies that either the catalytic ink composite induces changes in the geometry of the electrode surface, deviating from the linear behavior of the K-L plots [70], or some of the H₂O₂ initially produced at the disk surface is decomposed before reaching the Pt ring, which could be due to the 3D structure at the electrode surface. Thus, the presence of mononuclear sites that promote the H₂O₂ generation in CuL1 and CuL2 does not strongly affect the selectivity for ORR, since, for both catalysts, the number of electrons transferred is close to 4, following a direct 4 electrons electroreduction to water for the CuL1 catalyst and a 2e⁻ x 2e⁻ reaction pathway for the CuL2 catalyst.

To gain deep insight into the mechanism, Tafel slopes were calculated from the rotating disk currents corrected by the diffusional limiting current. Fig. 2a shows the Tafel plots calculated for the CuL1 and CuL2 catalysts. Both Tafel slopes are parallels and present values close to 0.120 V dec⁻¹ (Table 1), suggesting that the rate-limiting step is the same for both catalysts, corresponding to the first electron transfer concerted with the binding oxygen molecule on the binuclear Cu(I) active sites:



The proposed mechanism implies a concerted step of the first electron transfer with the binding mode of O₂ on a binuclear Cu(I) active site. Taking into consideration that mechanism, the current of the reaction can be expressed as the contribution of two driven forces: the electron transfer part, which is dependent on the applied potential, and the adsorption energy of O₂ molecules on binuclear Cu(I) centers, as has been previously proposed for other active MN4 complexes for the ORR

Table 1

Electrochemical parameters obtained from cyclic voltammetry and polarization curves for ORR on the CuL1 and CuL2 catalysts modified GC electrodes under convective conditions ($\omega = 1600$ rpm).

| Catalyst | E ^o _(I) (V vs. RHE) | E _{onset} (V vs. RHE) | Γ _{cat} (mol cm ⁻²) | Tafel slope | n ^o of e ⁻ RRDE (n) (at 0 V vs RHE) |
|----------|---|--------------------------------|--|-------------|---|
| CuL1 | 0.562 | 0.650 | 3.9 × 10 ⁻⁸ | -0.111 | 3.85 |
| CuL2 | 0.570 | 0.633 | 6.3 × 10 ⁻⁸ | -0.121 | 3.87 |

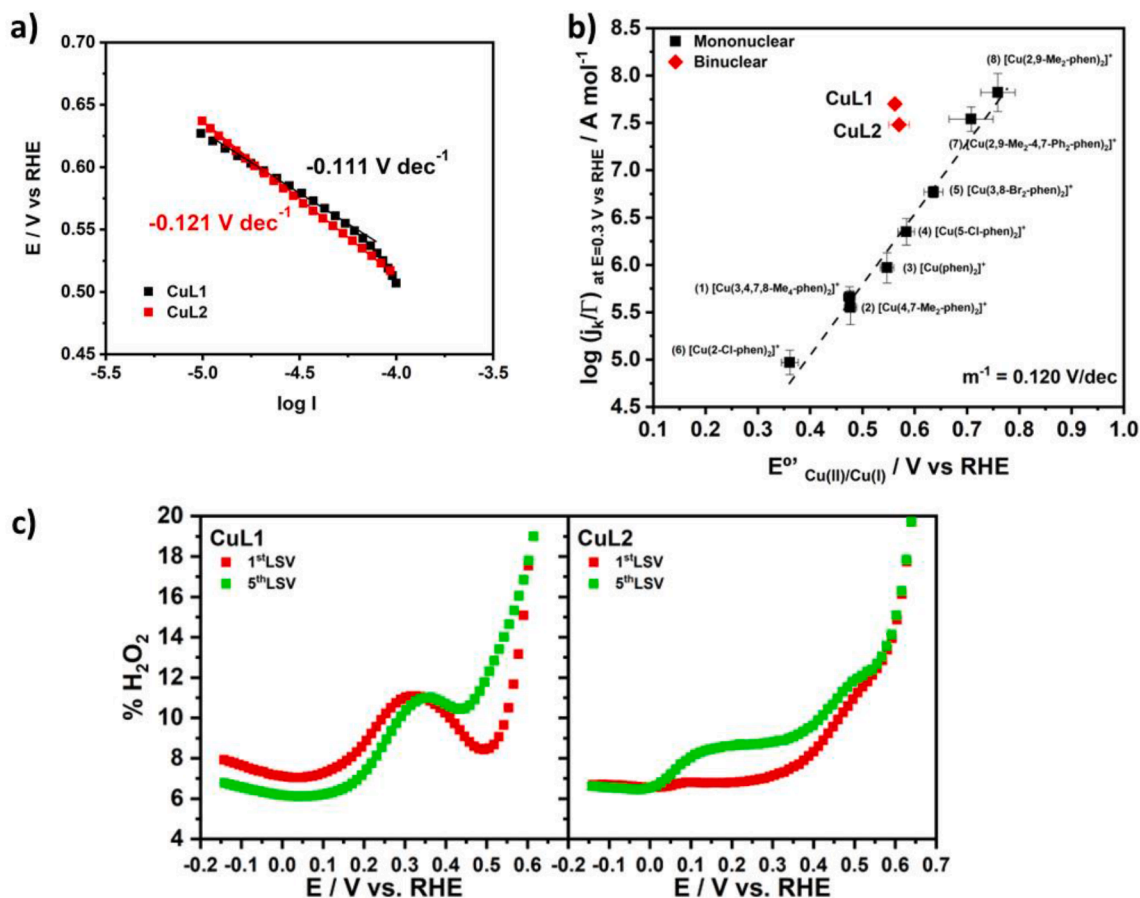


Fig. 2. (a) Tafel plots for ORR on GC electrodes modified with CuL1 (black squares) and CuL2 (red squares) catalysts obtained from LSV corrected by limiting currents. (b) Comparison of the catalytic activity obtained for CuL1 and CuL2 catalysts, expressed as $\log(j_k/r)$ versus E^0_{cat} and the correlation of $[Cu(phen)_2]^+$ derivatives for ORR obtained from [6]. (c) H_2O_2 production from CuL1 and CuL2 catalysts calculated from disk and ring currents displayed at 1600 rpm at the first and the fifth consecutive LSV.

[7,28,71].

Considering the voltammograms, since the electrogeneration of Cu(I) is potential dependent, the catalytic activity was evaluated as $\log j$ at a constant potential, by the extrapolation from the Tafel slopes and normalized by the total active sites determined by CV ($\log j/\Gamma$ at $E_{app} = 0.3$ V vs. RHE). Thus, the catalytic activity versus the redox potential of the binuclear complexes is represented in Fig. 2b and also compared with other mononuclear copper complexes previously published in the literature [6]. The binuclear Cu active sites present an increase in their electrocatalytic activity close to two orders of magnitude regarding the mononuclear Cu-complexes with similar redox potential, indicating the better performance of the binuclear catalysts for the ORR. Moreover, from a general comparison of the catalytic activity ($\log j/\Gamma$ at $E_{app} = 0.3$ V vs. RHE) versus the E^0 (M^{n+}/M^n) with previously reported MN4 molecular systems [6,71,72] (Figure S9), it can be noted that CuL1 and CuL2 fall in the activity ranges of classical systems as cobalt porphyrins (CoP) and iron phthalocyanines (FePc), showing that the influence of the synthesized ligands anchoring adjacent Cu centers play a fundamental role in increasing the E^0 (M^{n+}/M^n) and, therefore, their catalytic activity towards the ORR.

After the polarization tests, an extra polarization curve was performed to evaluate the changes in activity and H_2O_2 production. Figure S8 shows the first and the fifth polarization curve for both catalysts. As can be observed, the onset potential remains unaltered after the polarization tests, which inform of the good stability of the catalyst. However, there is a change in the H_2O_2 generation, mainly for the CuL2 catalysts, as can be observed in Fig. 2c, where the ring currents of the first and fifth polarization curves are compared. For the CuL1 catalyst,

there is an increase in the H_2O_2 production in the region of low overpotentials at the fifth scan, which could inform of a mixing mechanism of direct 4-electron reduction and a $2e^- \times 2e^-$ mechanism. Nevertheless, the ring currents for the CuL2 catalyst increase during the whole potential window evaluated, but this increase is more relevant at high overpotentials as shown in Fig. 2c. Despite the catalytic activity evaluated from the onset potential remaining unchanged, the increase in H_2O_2 production during consecutive polarization tests could be detrimental to the stability of the catalysts in long-term operando conditions.

To compare the catalytic activity and stability of the studied Cu-based catalysts under potentiostatic operating conditions, local measurements of the current response towards ORR were performed by SECM operating in the pumped-MD/SC mode. Fig. 3a shows the local activity quantification of the CuL1 catalyst by SECM as a function of the applied potential. This was conducted with the micropipette individually addressing the CuL1 catalytic spot in static mode and performing a chronoamperometry for 270 s, which was divided in 3 zones of 90 s each (identified by vertical dashed lines in Fig. 3a). The first and third zones correspond to the background current ($I_{background}$), where the micropipette is not delivering any O_2 in solution and the syringe pump is turned off. In contrast, the second zone corresponds to the ORR activity at the catalytic spot (I_{ORR}) under ORR steady-state conditions. The quantitative ORR current (ΔI) associated with the activity of both CuL1 and CuL2 catalytic spots is represented in Fig. 3b for comparing the behavior of the two Cu-based complexes synthesized. It is noteworthy that both Cu-based catalytic spots exhibit a very similar behavior for the ORR in the range of potentials where the chronoamperometries were conducted. Thus, the ligand structure does not seem to play a major role in the

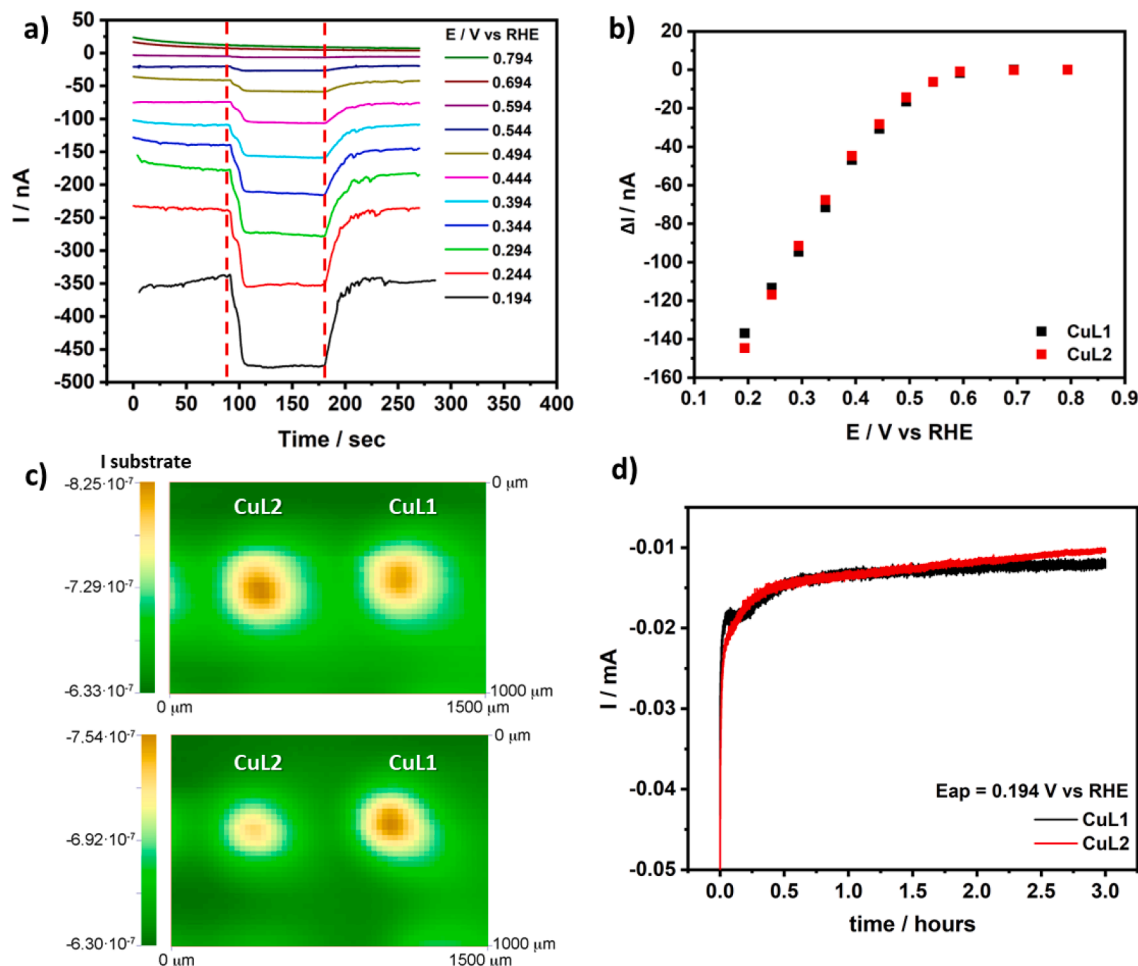


Fig. 3. (a) ORR activity quantification of the CuL1 catalyst by SECM in the pumped-MD/SC mode at different applied potentials. The micropipette-substrate distance was 50 μm , the micropipette diameter was 20 μm and the pumping flow was 55 $\mu\text{L h}^{-1}$. Solution composition: Ar-saturated 0.1 M NaClO_4 and 0.04 M Britton-Robinson buffer solution at pH 5.0. (b) ORR collected current response (ΔI) on both catalytic spots (CuL1) and (CuL2) (c) SECM imaging in the pumped-MD/SC mode for ORR on CuL1 and CuL2 spots. Upper and lower panels correspond to the initial and after 3 h of ORR SECM images, respectively ($E_{\text{app}} = 0.194 \text{ V vs RHE}$). Solution composition: Ar-saturated 0.1 M NaClO_4 and 0.04 M Britton-Robinson buffer solution at pH 5.0. The micropipette-substrate distance was 50 μm , the micropipette diameter was 20 μm and the pumping flow was 55 $\mu\text{L h}^{-1}$. The micropipette tip scan rate was 125 $\mu\text{m s}^{-1}$, using increments of 25 μm each 0.2 s. d) CAs at 0.194 V vs. RHE of both CuL1 and CuL2 catalysts working during 3.0 h in an O_2 -saturated 0.1 M NaClO_4 and 0.04 M Britton-Robinson buffer solution at pH 5.0.

instantaneous activity of the Cu-based catalysts compared herein.

The stability of the two Cu-based catalysts was evaluated under identical operando conditions (scanning the same electrode area held at the same potential) by consecutive SECM images operating in the pumped-MD/SC mode. Fig. 3c shows the initial SECM image obtained at a constant potential ($E_{\text{app}} = 0.194 \text{ V vs RHE}$) by pumping a constant O_2 flow from the micropipette (upper panel in Fig. 3c) and another identical SECM image after 3 h of experiment (lower panel in Fig. 3c). Initially, both catalytic spots show very similar activities for ORR, but after three hours of ORR operation in the range from 0.194 to 0.794 V vs RHE, the CuL2 spot exhibits a 12% decrease in current with respect to the initial current displayed. The catalyst deactivation is less significant for the case of CuL1 spot, which exhibits a 7% loss of the initial current displayed. In both cases, the activity evolution after undergoing this accelerated aging test under ORR operating conditions is very satisfactory and shows that Cu catalysts containing pyridyl and pyridylmethyl ligands exhibit significant activity and stability. Fig. 3d shows independent CAs performed on each Cu-based catalyst during 3.0 h in an O_2 -saturated electrolyte solution at the same constant potential ($E_{\text{app}} = 0.194 \text{ V vs RHE}$). CAs in Fig. 3d confirm the SECM outcome, CuL1 exhibits a higher catalytic current than CuL2 after 3 h of ORR. SECM imaging and CA results prove the ligand structure-reactivity correlation, which becomes especially relevant for achieving long-term activity and

stability for ORR under high overpotential and current conditions.

4. Conclusions

We have studied the influence of the ligand structure and flexibility on the catalytic activity and stability of two multinuclear copper-based catalysts, CuL1 and CuL2, supported on carbon black for the ORR by comparing 2-pyridyl (L1) and 2-pyridylmethyl (L2) substituents. CuL1 and CuL2 were synthesized and characterized by electrochemical measurements, indicating the coexistence of mono- and bi-nuclear Cu active sites in the catalysts. The total number of electrons transferred is close to four for both catalysts. However, the ring currents inform of a direct 4-electron pathway for CuL1 and a $2e^- \times 2e^-$ mechanism for CuL2. In addition, an apparent increase in ring currents after five consecutive polarization tests is detected for CuL2 catalyst. Regarding the activity, the binuclear catalysts present an electroactivity two orders of magnitude higher than the mononuclear catalysts previously described in the literature under identical conditions.

Both Cu-based catalysts exhibit a very similar initial activity for the ORR evaluated by SECM and LSV under rotation. Thus, the ligand structure does not seem to play a major role in the instantaneous activity. In contrast, the stability of both catalysts evaluated under ORR operating conditions by SECM imaging and CA demonstrated a

satisfactory performance. However, a higher decrease in catalytic activity under operando conditions was shown by CuL2 than CuL1. The increase in H₂O₂ production displayed by CuL2 in RRDE upon increasing the number of ORR polarization curves is probably responsible for the degradation of its catalytic activity. Based on these results, the extra flexibility conferred by the methyl group in CuL2 (pyridylmethyl ligand) is detrimental for the stability of the catalyst, since it promotes the electroreduction of dioxygen via 2e⁻ x 2e⁻ mechanism and enhances the electrogeneration of H₂O₂ during ORR. The degradation mechanism is unclear but could be associated with the direct corrosion of the carbon support and catalyst or via Fenton's reaction on copper sites. In conclusion, more rigid pyridyl ligands (CuL1) provide a more stable catalytic activity evolution under ORR operating conditions than flexible pyridylmethyl ligands (CuL2). This is the base for the future development of new Cu-based catalytic compounds with higher activity since their formal potential and, in consequence, the catalytic activity of [Cu(R-L1)] compounds can be modulated by substitution of 2-pyridyl groups containing electron-withdrawing substituents.

CRedit authorship contribution statement

Ricardo Venegas: Methodology, Validation, Formal analysis, Data curation, Writing – original draft, Writing – review & editing. **Karina Muñoz-Becerra:** Methodology, Formal analysis, Writing – original draft, Writing – review & editing. **Sophie Juillard:** . **Lin Zhang:** . **Rubén Oñate:** Formal analysis. **Ingrid Ponce:** Project administration, Funding acquisition. **Vincent Vivier:** Writing – review & editing. **Francisco J. Recio:** Methodology, Validation, Investigation, Resources, Writing – original draft, Writing – review & editing, Visualization, Supervision, Project administration, Funding acquisition. **Carlos M. Sánchez-Sánchez:** Methodology, Validation, Investigation, Resources, Writing – original draft, Writing – review & editing, Visualization, Supervision, Project administration, Funding acquisition.

Declaration of Competing Interest

The authors declare that they have no known competing financial interests or personal relationships that could have appeared to influence the work reported in this paper.

Data Availability

Data will be made available on request.

Acknowledgments

This work has been supported by ECOS Sud-Chile CONICYT program (Project C17E10/170037), FONDECYT Project 1161117, FONDECYT Project 11221073, FONDECYT Postdoctoral Project 3170330, and ACT192175. S. Juillard thanks Sorbonne Université for the PhD contract. L. Zhang thanks the PhD contract obtained in the frame of the joint program (Sorbonne Université - China Scholarship Council). The authors acknowledge the support of the centre National de la Recherche Scientifique (CNRS).

Supplementary materials

Supplementary material associated with this article can be found, in the online version, at [doi:10.1016/j.electacta.2022.141304](https://doi.org/10.1016/j.electacta.2022.141304).

References

- [1] L. Osmieri, Q. Meyer, Recent advances in integrating platinum group metal-free catalysts in proton exchange membrane fuel cells, *Curr. Opin. Electrochem.* 31 (2022), 100847, <https://doi.org/10.1016/j.coelec.2021.100847>.
- [2] K. Muñoz-Becerra, R. Venegas, L. Duque, J.H. Zagal, F.J. Recio, Recent advances of Fe–N–C pyrolyzed catalysts for the oxygen reduction reaction, *Curr. Opin. Electrochem.* 23 (2020) 154–161, <https://doi.org/10.1016/j.coelec.2020.08.006>.
- [3] Y.M. Zhao, G.Q. Yu, F.F. Wang, P.J. Wei, J.G. Liu, Bioinspired transition-metal complexes as electrocatalysts for the oxygen reduction reaction, *Chem. Eur. J.* 25 (2019) 3726–3739, <https://doi.org/10.1002/chem.201803764>.
- [4] J.H. Zagal, M.T.M. Koper, Reactivity descriptors for the activity of molecular MN₄ catalysts for the oxygen reduction reaction, *Angew. Chem. Int. Ed.* 55 (2016) 14510–14521, <https://doi.org/10.1002/anie.201604311>.
- [5] X. Li, H. Lei, L. Xie, N. Wang, W. Zhang, R. Cao, Metalloporphyrins as catalytic models for studying hydrogen and oxygen evolution and oxygen reduction reactions, *Acc. Chem. Res.* 55 (2022) 878–892, <https://doi.org/10.1021/acs.accounts.1c00753>.
- [6] R. Venegas, K. Muñoz-Becerra, L. Lemus, A. Toro-Labbé, J.H. Zagal, F.J. Recio, Theoretical and experimental reactivity predictors for the electrocatalytic activity of copper phenanthroline derivatives for the reduction of dioxygen, *J. Phys. Chem. C* 123 (2019) 19468–19478, <https://doi.org/10.1021/acs.jpcc.9b03200>.
- [7] J.H. Zagal, S. Griveau, J.F. Silva, T. Nyokong, F. Bedioui, Metallophthalocyanine-based molecular materials as catalysts for electrochemical reactions, *Coord. Chem. Rev.* 254 (2010) 2755–2791, <https://doi.org/10.1016/j.ccr.2010.05.001>.
- [8] M. Mahyari, S.E. Hooshmand, H. Sepahvand, J.N. Gavani, S.G. Hosseini, Biomimetic complexes-graphene composites for redox processes, *Appl. Organomet. Chem.* (2020) 34, <https://doi.org/10.1002/aoc.5540>.
- [9] K. Muñoz-Becerra, J.H. Zagal, R. Venegas, F.J. Recio, Strategies to improve the catalytic activity and stability of bioinspired Cu molecular catalysts for the ORR, *Curr. Opin. Electrochem.* (2022), 101035, <https://doi.org/10.1016/j.coelec.2022.101035>.
- [10] E.I. Solomon, P. Chen, M. Metz, S.-K. Lee, A.E. Palmer, Oxygen binding, activation, and reduction to water by copper proteins, *Angew. Chem. Int. Ed.* 40 (2001) 4570–4590, [10.1002/1521-3773\(20011217\)40:24<4570::AID-ANIE4570>3.0.CO;2-4](https://doi.org/10.1002/1521-3773(20011217)40:24<4570::AID-ANIE4570>3.0.CO;2-4).
- [11] N. Mano, V. Soukharev, A. Heller, A Laccase-wiring redox hydrogel for efficient catalysis of O₂ electroreduction, *J. Phys. Chem. B* 110 (2006) 11180–11187, <https://doi.org/10.1021/jp055654e>.
- [12] E.I. Solomon, A.J. Augustine, J. Yoon, O₂ reduction to H₂O by the multicopper oxidases, *Dalton Trans.* 30 (2008) 3921, <https://doi.org/10.1039/b800799c>.
- [13] M.S. Thorum, C.A. Anderson, J.J. Hatch, A.S. Campbell, N.M. Marshall, S. C. Zimmerman, Y. Lu, A.A. Gewirth, Direct, electrocatalytic oxygen reduction by Laccase on anthracene-2-methanethiol-modified gold, *J. Phys. Chem. Lett.* 1 (2010) 2251–2254, <https://doi.org/10.1021/jz100745s>.
- [14] C.E. Elwell, N.L. Gagnon, B.D. Neisen, D. Dhar, A.D. Spaeth, G.M. Yee, W. B. Tolman, Copper-oxygen complexes revisited: structures, spectroscopy, and reactivity, *Chem. Rev.* 117 (2017) 2059–2107, <https://doi.org/10.1021/acs.chemrev.6b00636>.
- [15] Y. Lei, F.C. Anson, Mechanistic aspects of the electroreduction of dioxygen as catalyzed by copper-phenanthroline complexes adsorbed on graphite electrodes, *Inorg. Chem.* 33 (1994) 5003–5009, <https://doi.org/10.1021/ic00100a026>.
- [16] C.C.L. McCrory, X. Ottenwaelde, T.D.P. Stack, C.E.D. Chidsey, Kinetic and mechanistic studies of the electrocatalytic reduction of O₂ to H₂O with mononuclear Cu complexes of substituted 1,10-phenanthrolines, *J. Phys. Chem. A* 111 (2007) 12641–12650, <https://doi.org/10.1021/jp076106z>.
- [17] M. Langerman, D.G.H. Hetterscheid, Fast oxygen reduction catalyzed by a copper (II) tris(2-pyridylmethyl)amine complex through a stepwise mechanism, *Angew. Chem. Int. Ed.* 58 (2019) 12974–12978, <https://doi.org/10.1002/anie.201904075>.
- [18] M. Asahi, S. Yamazaki, S. Itoh, T. Ioroi, Acid-base and redox equilibria of a tris(2-pyridylmethyl)amine copper complex; their effects on electrocatalytic oxygen reduction by the complex, *Electrochim. Acta* 211 (2016) 193–198, <https://doi.org/10.1016/j.electacta.2016.05.166>.
- [19] M.A. Thorseth, C.E. Tornow, E.C.M. Tse, A.A. Gewirth, Cu complexes that catalyze the oxygen reduction reaction, *Coord. Chem. Rev.* 257 (2013) 130–139, <https://doi.org/10.1016/j.ccr.2012.03.033>.
- [20] K.W. Hipps, X. Lu, X.D. Wang, U. Mazur, Metal d-orbital occupation-dependent images in the scanning tunneling microscopy of metal phthalocyanines, *J. Phys. Chem.* 100 (1996) 11207–11210, <https://doi.org/10.1021/jp960422o>.
- [21] I. Ponce, J.F. Silva, R. Oñate, M.C. Rezende, M.A. Paez, J.H. Zagal, J. Pavez, F. Mendizabal, S. Miranda-Rojas, A. Muñoz-Castro, R. Arratia-Pérez, Enhancement of the catalytic activity of Fe phthalocyanine for the reduction of O₂ anchored to Au(111) via conjugated self-assembled monolayers of aromatic thiols as compared to Cu phthalocyanine, *J. Phys. Chem. C* 116 (2012) 15329–15341, <https://doi.org/10.1021/jp301093q>.
- [22] Z. Ma, Y. Chu, C. Fu, H. Du, X. Huang, J. Zhao, The effects of coordinated molecules of two Gly-Schiff base copper complexes on their oxygen reduction reaction performance, *Catalysts* 8 (2018), <https://doi.org/10.3390/catal8040156>.
- [23] R. Davydov, A.E. Herzog, R.J. Jodts, K.D. Karlin, B.M. Hoffman, End-on copper(II) superoxo and Cu(II) peroxo and hydroperoxo complexes generated by cryoreduction/annealing and characterized by EPR/ENDOR spectroscopy, *J. Am. Chem. Soc.* 144 (2022) 377–389, <https://doi.org/10.1021/jacs.1c10252>.
- [24] N.W.G. Smits, B. van Dijk, I. de Bruin, S.L.T. Groeneveld, M.A. Siegler, D.G. H. Hetterscheid, Influence of ligand denticity and flexibility on the molecular copper mediated oxygen reduction reaction, *Inorg. Chem.* 59 (2020) 16398–16409, <https://doi.org/10.1021/acs.inorgchem.0c02204>.
- [25] C.A. Gutierrez, J.F. Silva, F.J. Recio, S. Griveau, F. Bedioui, C.A. Caro, J.H. Zagal, In search of the best iron N₄-macrocyclic catalysts adsorbed on graphite electrodes and on multi-walled carbon nanotubes for the oxidation of L-Cysteine by adjusting the Fe(II)/(I) formal potential of the complex, *Electrocatalysis* 5 (2014) 426–437, <https://doi.org/10.1007/s12678-014-0209-y>.

- [26] M.A. Gulppi, F.J. Recio, F. Tasca, G. Ochoa, J.F. Silva, J. Pavez, J.H. Zagal, Optimizing the reactivity of surface confined cobalt N4-macrocyclics for the electrocatalytic oxidation of L-cysteine by tuning the Co(II)/(I) formal potential of the catalyst, *Electrochim. Acta* 126 (2014) 37–41, <https://doi.org/10.1016/j.electacta.2013.07.230>.
- [27] F.J. Recio, C.A. Gutierrez, R. Venegas, C. Linares-Flores, C.A. Caro, J.H. Zagal, Optimization of the electrocatalytic activity of MN4-macrocyclics adsorbed on graphite electrodes for the electrochemical oxidation of L-cysteine by tuning the M (II)/(I) formal potential of the catalyst: an overview, *Electrochim. Acta* 140 (2014) 482–488, <https://doi.org/10.1016/j.electacta.2014.04.098>.
- [28] J.H. Zagal, F.J. Recio, C.A. Gutierrez, C. Zúñiga, M.A. Páez, C.A. Caro, Towards a unified way of comparing the electrocatalytic activity MN4 macrocyclic metal catalysts for O₂ reduction on the basis of the reversible potential of the reaction, *Electrochem. Commun.* 41 (2014) 24–26, <https://doi.org/10.1016/j.elecom.2014.01.009>.
- [29] M.S. Thorum, J. Yadav, A.A. Gewirth, Oxygen reduction activity of a copper complex of 3,5-diamino-1,2,4-triazole supported on carbon black, *Angew. Chem. Int. Ed.* 48 (2009) 165–167, <https://doi.org/10.1002/anie.200803554>.
- [30] Y.T. Xi, P.J. Wei, R.C. Wang, J.G. Liu, Bio-inspired multinuclear copper complexes covalently immobilized on reduced graphene oxide as efficient electrocatalysts for the oxygen reduction reaction, *Chem. Comm.* 51 (2015) 7455–7458, <https://doi.org/10.1039/C5CC00963D>.
- [31] N. Thiagarajan, D. Janmachi, Y.-F.F. Tsai, W.H. Wana, R. Ramu, S.I. Chan, J.M. M. Zen, S.S.F. Yu, A carbon electrode functionalized by a tricopper cluster complex: overcoming overpotential and production of hydrogen peroxide in the oxygen reduction reaction, *Angew. Chem.* 130 (2018) 3674–3678, <https://doi.org/10.1002/ange.201712226>.
- [32] S. Gentil, J.K. Molloy, M. Carrière, G. Gellon, C. Philouze, D. Serre, F. Thomas, A. le Goff, Substituent effects in carbon-nanotube-supported copper phenolato complexes for oxygen reduction reaction, *Inorg. Chem.* 60 (2021) 6922–6929, <https://doi.org/10.1021/acs.inorgchem.1c00157>.
- [33] E.C.M. Tse, D. Schilter, D.L. Gray, T.B. Rauchfuss, A.A. Gewirth, Multicopper models for the laccase active site: effect of nuclearity on electrocatalytic oxygen reduction, *Inorg. Chem.* 53 (2014) 8505–8516, <https://doi.org/10.1021/ic501080c>.
- [34] F.R. Brushett, M.S. Thorum, N.S. Lioutas, M.S. Naughton, C. Tornow, H.R. M. Jhong, A.A. Gewirth, P.J.A. Kenis, A carbon-supported copper complex of 3,5-diamino-1,2,4-triazole as a cathode catalyst for alkaline fuel cell applications, *J. Am. Chem. Soc.* 132 (2010) 12185–12187, <https://doi.org/10.1021/ja104767w>.
- [35] B. Li, Y. Peng, G. Li, J. Hua, Y. Yu, D. Jin, Z. Shi, S. Feng, Design and construction of coordination polymers by 4-amino-3,5-bis(*n*-pyridyl)-1,2,4-triazole (*n* = 2, 3, 4) isomers in a copper(I) halide system: diverse structures tuned by isomeric and anion effects, *Cryst. Growth Des.* 10 (2010) 2192–2201, <https://doi.org/10.1021/cg901438x>.
- [36] N.G. White, J.A. Kitchen, J.A. Joulé, S. Brooker, Copper-induced N–N bond cleavage results in an octanuclear expanded-core grid-like complex, *Chem. Comm.* 48 (2012) 6229, <https://doi.org/10.1039/c2cc32018e>.
- [37] C. Ai-Hua, M. Su-Ci, Z. Kai, W. Cong-Cong, Z. Wei, W. Ai-Jian, Q. Jun, A new copper(I) complex based on 4-amino-3,5-bis(3-pyridyl)-1,2,4-triazole: synthesis, crystal structure, theoretical study, thermal behavior and luminescence, *J. Chem. Sci.* 129 (2017) 185–191, <https://doi.org/10.1007/s12039-017-1226-1>.
- [38] M. Klingele, S. Brooker, The coordination chemistry of 4-substituted 3,5-di(2-pyridyl)-4H-1,2,4-triazoles and related ligands, *Coord. Chem Rev.* 241 (2003) 119–132, [https://doi.org/10.1016/S0010-8545\(03\)00049-3](https://doi.org/10.1016/S0010-8545(03)00049-3).
- [39] M.H. Klingele, P.D.W. Boyd, B. Moubaraki, K.S. Murray, S. Brooker, First complexes of a 4-alkyl-3,5-di(2-pyridyl)-4H-1,2,4-triazole: synthesis, X-ray crystal structures and magnetic properties of dinuclear cobalt(II), nickel(II) and copper(II) complexes of 4-isobutyl-3,5-di(2-pyridyl)-4H-1,2,4-triazole, *Eur. J. Inorg. Chem.* (2005) 910–918, <https://doi.org/10.1002/ejic.200400780>.
- [40] P. Martín-Ramos, M.R. Silva, J. de A. e Silva, N.D. Martins, C. Yuste-Vivas, P. S. Pereira da Silva, A.J.F.N. Sobral, L.C.J. Pereira, Synthesis, structure and magnetic properties of mono-, dinuclear and polymeric compounds of transition metals with 4-amino-3,5-di-pyridyl-4H-1,2,4-triazole, *J. Mol. Struct.* 1108 (2016) 278–287, <https://doi.org/10.1016/j.molstruc.2015.12.024>.
- [41] A.J. Bard, M. v. Mirkin, *Scanning Electrochemical Microscopy*, CRC Press, 2012, <https://doi.org/10.1201/b11850>.
- [42] C.M. Sánchez-Sánchez, Studying electrocatalytic activity using scanning electrochemical microscopy, *Electrochem. Soc. Interface* 23 (2014) 43–45, <https://doi.org/10.1149/2.F04142if>.
- [43] D. Polcar, P. Dauphin-Ducharme, J. Mauzeroll, Scanning electrochemical microscopy: a comprehensive review of experimental parameters from 1989 to 2015, *Chem. Rev.* 116 (2016) 13234–13278, <https://doi.org/10.1021/acs.chemrev.6b00067>.
- [44] C.M. Sánchez-Sánchez, J. Solla-Gullón, J. Montiel, R.G. Compton, J.D. Wadhawan, *Electrocatalysis at nanoparticles. Nanosystems Electrochemistry*, RSC Publishing, Cambridge, 2013, pp. 34–70, <https://doi.org/10.1039/9781849734820-00034>.
- [45] C.G. Zoski, Review — advances in scanning electrochemical microscopy (SECM), *J. Electrochem. Soc.* 163 (2016) 3088–3100, <https://doi.org/10.1149/2.0141604jes>.
- [46] J.L. Fernández, A.J. Bard, Scanning electrochemical microscopy. 47. Imaging electrocatalytic activity for oxygen reduction in an acidic medium by the tip generation - Substrate collection mode, *Anal. Chem.* 75 (2003) 2967–2974, <https://doi.org/10.1021/ac0340354>.
- [47] Y. Shen, M. Träuble, G. Wittstock, Detection of hydrogen peroxide produced during electrochemical oxygen reduction using scanning electrochemical microscopy, *Anal. Chem.* 80 (2008) 750–759, <https://doi.org/10.1021/ac0711889>.
- [48] K. Eckhard, W. Schuhmann, Localised visualisation of O₂ consumption and H₂O₂ formation by means of SECM for the characterisation of fuel cell catalyst activity, *Electrochim. Acta* 53 (2007) 1164–1169, <https://doi.org/10.1016/j.electacta.2007.02.028>.
- [49] C.M. Sánchez-Sánchez, A.J. Bard, Hydrogen peroxide production in the oxygen reduction reaction at different electrocatalysts as quantified by scanning electrochemical microscopy, *Anal. Chem.* 81 (2009) 8094–8100, <https://doi.org/10.1021/ac901291v>.
- [50] J.L. Fernández, D.A. Walsh, A.J. Bard, Thermodynamic guidelines for the design of bimetallic catalysts for oxygen electroreduction and rapid screening by scanning electrochemical microscopy. M-Co (M: Pd, Ag, Au), *J. Am. Chem. Soc.* 127 (2005) 357–365, <https://doi.org/10.1021/ja0449729>.
- [51] C.M. Sánchez-Sánchez, J. Solla-Gullón, F.J. Vidal-Iglesias, A. Aldaz, V. Montiel, E. Herrero, Imaging structure sensitive catalysis on different shape-controlled platinum nanoparticles, *J. Am. Chem. Soc.* 132 (2010) 5622–5624, <https://doi.org/10.1021/ja100922h>.
- [52] J.V. Perales-Rondón, E. Herrero, J. Solla-Gullón, C.M. Sánchez-Sánchez, V. Vivier, Oxygen crossover effect on palladium and platinum based electrocatalysts during formic acid oxidation studied by scanning electrochemical microscopy, *J. Electroanal. Chem.* 793 (2017) 218–225, <https://doi.org/10.1016/j.jelechem.2016.12.049>.
- [53] N. Limani, A. Boudet, N. Blanchard, B. Jousselmé, R. Cornut, Local probe investigation of electrocatalytic activity, *Chem. Sci.* 12 (2021) 71–98, <https://doi.org/10.1039/D0SC04319B>.
- [54] A.O. Okunola, T.C. Nagaiah, X. Chen, K. Eckhard, W. Schuhmann, M. Bron, Visualization of local electrocatalytic activity of metalloporphyrins towards oxygen reduction by means of redox competition scanning electrochemical microscopy (RC-SECM), *Electrochim. Acta* 54 (2009) 4971–4978, <https://doi.org/10.1016/j.electacta.2009.02.047>.
- [55] J. Noel, N. Kostopoulos, C. Achaibou, C. Fave, E. Anxolabéhère-Mallart, F. Kanoufi, Probing the activity of iron peroxo porphyrin intermediates in the reaction layer during the electrochemical reductive activation of O₂, *Angew. Chem. Int. Ed.* 59 (2020) 16376–16380, <https://doi.org/10.1002/anie.202004977>.
- [56] A. Dobrzyniecka, A. Zeradjanin, J. Masa, A. Puschhof, J. Stroka, P.J. Kulesza, W. Schuhmann, Application of SECM in tracing of hydrogen peroxide at multicomponent non-noble electrocatalyst films for the oxygen reduction reaction, *Catal. Today* 202 (2013) 55–62, <https://doi.org/10.1016/j.cattod.2012.03.060>.
- [57] S. Srinivas, A. Senthil Kumar, High-performance electrocatalytic reduction and sensing of hazardous hexavalent chromium using a redox-active binol species-impregnated carbon nanofiber-modified electrode, *J. Phys. Chem. C* 126 (2022) 8296–8311, <https://doi.org/10.1021/acs.jpcc.2c00317>.
- [58] J.-M. Noël, F. Kanoufi, Probing the reactive intermediate species generated during electrocatalysis by scanning electrochemical microscopy, *Curr. Opin. Electrochem.* 35 (2022), 101071, <https://doi.org/10.1016/j.coelec.2022.101071>.
- [59] N. Aouina, F. Balbaud-Célériér, F. Huet, S. Joiret, H. Perrot, F. Rouillard, V. Vivier, A flow microdevice for studying the initiation and propagation of a single pit, *Corros. Sci.* 62 (2012) 1–4, <https://doi.org/10.1016/j.corsci.2012.05.002>.
- [60] N. Aouina, F. Balbaud-Célériér, F. Huet, S. Joiret, H. Perrot, F. Rouillard, V. Vivier, Initiation and growth of a single pit on 316L stainless steel: influence of SO₄²⁻ and ClO₄⁻ anions, *Electrochim. Acta* 104 (2013) 274–281, <https://doi.org/10.1016/j.electacta.2013.04.109>.
- [61] S. Heurtault, R. Robin, F. Rouillard, V. Vivier, Initiation and propagation of a single pit on stainless steel using a local probe technique, *Faraday Discuss* 180 (2015) 267–282, <https://doi.org/10.1039/C4FD000252K>.
- [62] S. Heurtault, R. Robin, F. Rouillard, V. Vivier, On the propagation of open and covered pit in 316L stainless steel, *Electrochim. Acta* 203 (2016) 316–325, <https://doi.org/10.1016/j.electacta.2016.01.084>.
- [63] L. Cheng, W.-X. Zhang, B.-H. Ye, J. Lin, X. Chen, In situ solvothermal generation of 1,2,4-triazoles and related compounds from organonitrile and hydrazine hydrate: a mechanism study, *Inorg. Chem.* 46 (2007) 1135–1143, <https://doi.org/10.1021/ic061303i>.
- [64] O. Lugaes, J.V. Perales-Rondón, A. Minguzzi, J. Solla-Gullón, S. Rondinini, J. M. Feliu, C.M. Sánchez-Sánchez, Rapid screening of silver nanoparticles for the catalytic degradation of chlorinated pollutants in water, *Appl. Catal. B* 163 (2015) 554–563, <https://doi.org/10.1016/j.apcatb.2014.08.030>.
- [65] Y.P. Kharwar, S. Mandal, K. Ramanujam, Carbon supported and nafion stabilized copper (II) based 1d coordination polymer as an electrocatalyst for oxygen reduction reaction, *J. Electrochem. Soc.* 166 (2019) F3193–F3201, <https://doi.org/10.1149/2.0221907jes>.
- [66] M. Kato, N. Oyaizu, K. Shimazu, I. Yagi, Oxygen reduction reaction catalyzed by self-assembled monolayers of copper-based electrocatalysts on a polycrystalline gold surface, *J. Phys. Chem. C* 120 (2016) 15814–15822, <https://doi.org/10.1021/acs.jpcc.5b11663>.
- [67] M.M.T. Khan, P. Paul, Electrochemical studies of dinuclear copper(I) complexes with ligands having N₂P₄ and N₂As₄ donor sites: generation of Cu^{II}-Cu^I mixed valence species, *Polyhedron* 11 (1992) 805–809, [https://doi.org/10.1016/S0277-5387\(00\)86014-3](https://doi.org/10.1016/S0277-5387(00)86014-3).
- [68] P. Mayuri, N. Saravanan, A. Senthil Kumar, A bioinspired copper 2,2-bipyridyl complex immobilized MWCNT modified electrode prepared by a new strategy for elegant electrocatalytic reduction and sensing of hydrogen peroxide, *Electrochim. Acta* 240 (2017) 522–533, <https://doi.org/10.1016/j.electacta.2017.04.082>.
- [69] J. Masa, C. Batchelor-McAuley, W. Schuhmann, R.G. Compton, Koutecky-Levich analysis applied to nanoparticle modified rotating disk electrodes: electrocatalysis or misinterpretation, *Nano Res.* 7 (2014) 71–78, <https://doi.org/10.1007/s12274-013-0372-0>.

- [70] R. Zhou, Y. Zheng, M. Jaroniec, S.-Z.Z. Qiao, Determination of the electron transfer number for the oxygen reduction reaction: from theory to experiment, *ACS Catal.* 6 (2016) 4720–4728, <https://doi.org/10.1021/acscatal.6b01581>.
- [71] R. Venegas, K. Muñoz-Becerra, C. Candia-Onfray, J.F. Marco, J.H. Zagal, F.J. Recio, Experimental reactivity descriptors of M-N-C catalysts for the oxygen reduction reaction, *Electrochim. Acta* 332 (2020), 135340, <https://doi.org/10.1016/j.electacta.2019.135340>.
- [72] R. Venegas, F.J. Recio, J. Riquelme, K. Neira, J.F. Marco, I. Ponce, J.H. Zagal, F. Tasca, Biomimetic reduction of O₂ in an acid medium on iron phthalocyanines axially coordinated to pyridine anchored on carbon nanotubes, *J. Mater. Chem. A* 5 (2017) 12054–12059, <https://doi.org/10.1039/C7TA02381B>.